*Int. J. Therm. Sci.* (2000) 39, 771–779

S1290-0729(00)00270-2/FLA

# Investigation of heat transfer from circular cylinders in high power 10 kHz and 20 kHz acoustic resonant fields

Volker Uhlenwinkel [a]*, Rongxiang Meng [b], Klaus Bauckhage [a]

[a] *University of Bremen, Process Engineering, FB4, FG1, Badgasteiner Str. 3, D-28359 Bremen, Germany*

[b] *Institute for Material Science, Badgasteiner Str. 3, D-28359 Bremen, Germany*

(Received 3 February 1999, accepted 31 January 2000)

**Abstract** — This paper reports on the experimental results of heat transfer in 10 and 20 kHz acoustic resonant standing wave fields for a small cylinder by means of hot-film anemometry. To obtain the high power 10 and 20 kHz acoustic resonant standing wave fields, pairs of oscillating transmitters, each working with slightly different frequencies, were employed. It is shown that the effective sound pressure depends on several parameters like the irradiation number, the amplitude of the transmitters, the impedance, and the frequency. An empirical equation is given to calculate the effective sound pressure in the acoustic standing wave field. A remarkable enhancement of the heat transfer can be observed in the acoustic field compared to free convection. Finally, a correlation is given to predict the heat transfer in such acoustic fields. This correlation is valid for a wide range of Reynolds numbers (4–3 000). © 2000 Éditions scientifiques et médicales Elsevier SAS

**heat transfer / oscillating flow / acoustic standing wave / hot wire anemometry**

**Résumé** — **Influence de champs acoustiques résonants de grande puissance à 10 et 20 kHz sur le transfert de chaleur à partir de cylindres circulaires.** Cet article rend compte des résultats relatifs aux transferts de chaleur d'un cylindre de petit diamètre, dans un champ d'ondes acoustiques de 10 et 20 kHz en résonances. Ces résultats furent obtenus par l'intermédiaire d'un film chaud anémométrique. Afin d'obtenir la haute puissance de 10 et 20 kHz en résonance, deux transmetteurs à oscillations, travaillant à des fréquences légèrement différentes, furent employés. Il a été montré que la pression acoustique effective dépend de plusieurs paramètres tels que le nombre d'irradiation, l'amplitude des deux transmetteurs, l'impédance et la fréquence. Une relation empirique a été étable pour calculer cette pression dans le champ précédemment mentionné. Une amélioration notable du transfert de chaleur dans un tel champ en comparaison avec la convection libre peut être observée. Finalement, une corrélation est donnée afin de prédire le transfert de chaleur dans de ces champs acoustiques. Cette corrélation reste valide sur un large intervalle de nombre de Reynolds (de 4 à 3 000). © 2000 Éditions scientifiques et médicales Elsevier SAS

**transfert de chaleur / flux oscillant / onde acoustique / anémométrie à film chaud**

## Nomenclature

| | | |
|---|---|---|
| $A$ | surface area of the hot-film/wire probe | $m^{-2}$ |
| $B$ | calibration constant (equation (3)) | |
| $c$ | speed of sound (sound velocity) | $m{\cdot}s^{-1}$ |
| $c_0$ | speed of sound at normal temperature | $m{\cdot}s^{-1}$ |
| $D$ | transmitter diameter | m |
| $d$ | hot-film/wire probe diameter | m |
| $f$ | frequency | $s^{-1}$ |
| $h$ | heat transfer coefficient | $W{\cdot}m^{-2}{\cdot}K^{-1}$ |
| $k_1, k_2$ | constants (equation (13)) | |
| $k$ | thermal conductivity | $W{\cdot}m^{-1}{\cdot}K^{-1}$ |
| $\lambda$ | wavelength | m |
| $L$ | distance between the transmitters $= n\lambda/2$ | m |
| $l$ | length of the hot-film/wire probe | m |
| $m$ | calibration constant (equation (3)) | |
| $n$ | number of sound pressure nodes | |
| $Nu$ | Nusselt number | |
| $Nu_0$ | Nusselt number for free convection | |
| $p$ | effective sound pressure | $N{\cdot}m^{-2}$ |
| $P_{el}$ | electric power | W |
| $p_0$ | standard pressure | $N{\cdot}m^{-2}$ |
| $p_a$ | ambient pressure | $N{\cdot}m^{-2}$ |
| $Pr$ | Prandtl number | |
| $Re$ | Reynolds number | |
| $\dot{Q}$ | heat flow | W |
| $\dot{Q}_{conv}$ | heat flow due to convection | W |
| $\dot{Q}_{cond}$ | heat flow due to conduction | W |

* Correspondence and reprints.
uhl@iwt.uni-bremen.de

| | | |
|---|---|---|
| $\dot{Q}_{\mathrm{rad}}$ | heat flow due to radiation . . . . . | W |
| $R$ | resistance of the hot-film/wire probe . . | Ω |
| $T$ | operation temperature of the probe . . . | °C |
| $T_{\mathrm{a}}$ | ambient temperature . . . . . | °C |
| $u$ | mean gas velocity . . . . . | $\mathrm{m{\cdot}s^{-1}}$ |
| $U$ | voltage of the hot-film/wire probe . . . . | V |
| $U_0$ | voltage of the hot-film/wire probe due to free convection . . . . . | V |
| $v$ | effective sound particle velocity . . . . . | $\mathrm{m{\cdot}s^{-1}}$ |
| $v_{\mathrm{trans}}$ | effective velocity of the transmitter surface . . . . . | $\mathrm{m{\cdot}s^{-1}}$ |
| $\hat{v}_{\mathrm{trans}}$ | velocity amplitude of the transmitter surface . . . . . | $\mathrm{m{\cdot}s^{-1}}$ |
| $Y$ | displace amplitude of the transmitter . . | m |
| $Y^*$ | dimensionless displace amplitude of the transmitter $Y/Y_0$ with $Y_0 = 100$ µm | |
| $Z$ | specific acoustic impedance $= \rho c$ . . . . | $\mathrm{kg{\cdot}m^{-2}{\cdot}s^{-1}}$ |
| $Z^*$ | dimensionless impedance $V = Z/Z_{\mathrm{air}}$ | |
| $Z_{\mathrm{air}}$ | impedance of air at normal temperature and pressure . . . . . | $\mathrm{kg{\cdot}m^{-2}{\cdot}s^{-1}}$ |

*Greek symbols*

| | | |
|---|---|---|
| $\delta$ | correction value (equations (7), (8)) | |
| $\varphi$ | irradiation number | |
| $\eta$ | dynamic viscosity . . . . . | $\mathrm{N{\cdot}s{\cdot}m^{-2}}$ |
| $\lambda$ | wavelength . . . . . | m |
| $\rho$ | density . . . . . | $\mathrm{kg{\cdot}m^{-3}}$ |
| $\rho_0$ | normal density . . . . . | $\mathrm{kg{\cdot}m^{-3}}$ |

## 1. INTRODUCTION

There are several investigations published concerning the heat transfer on bodies in oscillating flows. In general, cylinders in a cross flow situation are used, because they are easier to handle than spheres. In the literature both simple harmonic flows and more complex flows with superimposed constant flow are also examined.

*Figure 1* gives an overview of the papers considered in this article. The different ranges of frequency and amplitude of the sound particle velocity are shown. A choice of the exact data together with the Reynolds number is summarized in *table I*. The range of the present study, which can also be found in *table I*, is different compared to the data of other papers. The frequency as well as the sound particle velocity show far higher values. Some authors give relations for the heat transfer, but these cannot be compared directly due to different definitions of the Reynolds number. For that reason only a few qualitative results from those papers are summarized as follows.

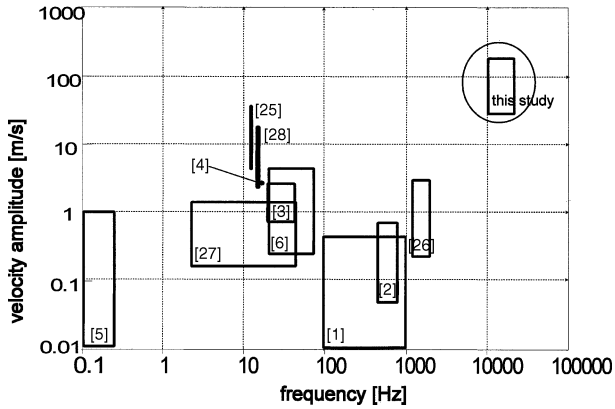


**Figure 1.** Frequency and velocity ranges of different papers dealing with heat transfer in oscillating flows.

TABLE I
Overview of the different parameter ranges of the considered papers.

| Author | Frequency range [Hz] | Velocity range [$\mathrm{m{\cdot}s^{-1}}$] | *Re* |
|---|---|---|---|
| Goldmann [1] | 100–1 000 | 0.003–0.45 | 0.004–0.15 |
| Müller [2] | 512–768 | 0.05–0.7 | 0.008–0.17 |
| Trasher [3] | 20–40 | up to 4 | – |
| Armaly [4] | up to 20 | up to 2.68 | 1–40 |
| Hutton [5] (in water) | up to 0.24 | 1 | up to 70 |
| Elger [6] | 25–70 | 0.2–5.6 | 0.03–0.64 |
| Bayazitoglu [7] | – | – | – |
| Present study | 10 000–20 000 | 30–130 | 4–3 000 |

If the velocity amplitude is used to calculate the Reynolds number in an oscillating flow, then the calculated heat transfer in the oscillating flow is generally lower than in a constant flow [1, 2, 4, 6, 7]. An increase of heat transfer can be achieved by an increase of the velocity amplitude. Both a higher frequency and a higher displacement amplitude lead to the necessary increase of the velocity amplitude [3, 4, 6, 7]. A decrease of the heat transfer is achieved by a higher freqency when the velocity amplitude remains constant [1, 2, 7]. Although the frequency is assumed to have an effect on the heat transfer, no investigation could be found considering a heat transfer correlation, in which the frequency is taken into account.

Armaly [4] successfully describes the heat transfer in an oscillating flow (for low frequencies) by using an equation valid for heat transfer of a constant flow with the effective velocity $v_{\mathrm{eff}}$ in the Reynolds number (instead of the velocity amplitude $v_{\mathrm{max}} = 1.41 v_{\mathrm{eff}}$).

All relations can only be used for mean values of the heat transfer and cannot be referred to when the heat transfer is to be presented as a function of time or when low frequencies are employed [7]. In these cases a time difference between the velocity and the heat transfer can be observed, with the heat transfer laging behind the velocity.

In accordance to the statements above, heat transfer correlations from other papers should not be used, if they are related to a different frequency range.

The acoustic field described in this paper is applied to atomize viscous fluids [8] and even molten metal [9–11]. The results can be used to calculate the solidification behavior of atomized particles. The results can also be applied to the levitation of solid particles or liquid droplets in basic research experiments. For this application it is important to know the heat and mass transfer conditions, which are investigated.

This paper is empirical in nature. Nevertheless, it should be mentioned that there are several papers focused on theoretical work on solving the boundary layer around a circular cylinder in oscillating flow [12–19].

## 2. EXPERIMENTAL SETUP AND MEASURING TECHNIQUE

The experimental setup can be subdivided into three parts:

- generation of the acoustic field;
- measuring of the sound pressure and the sound particle velocity, respectively;
- measuring of the heat transfer by hot-film or hot-wire anemometry.

A schematic overview of the setup is given in *figure 2*. The sound field is generated by two identical systems consisting of a transmitter (A1), booster, converter, and generator (A2). The transmitter surfaces (perpendicular to the $x$ axis) oscillate in $x$-direction. The sound pressure is measured by a sound pressure probe (B1), which transmits the signal to an amplifier (B2) and an analyser (B3). The signal of the hot-film/wire probe (C1) is connected to an anemometer (C2) and an analyser (C3). Technical data of the equipment is summarized in *table II*. The centre of the acoustic field is defined as the origin of the two-dimensional coordinate system ($x$- and $r$-axis). The components of the experimental setup will be illustrated in more detail in the following section.

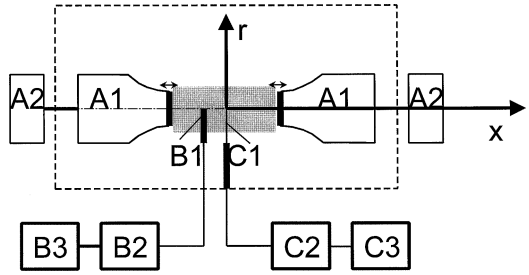


**Figure 2.** Schematic overview of the experimental setup.

TABLE II
Technical data of the equipment.

| | | |
|---|---|---|
| Sound pressure probe (piezoelectric) | Fa. Ziegler, model 105A03 | $p$ |
| Hot-film probe | TSI Typ 1210-20, $d = 51$ μm, $l = 1.00$ mm | $Nu$ |
| Hot-wire probe | TSI Typ 1520-T1,5; $d = 4$ μm, $l = 1.25$ mm | $Nu$ |
| Hot-wire probe | Dantec Typ 55-P11; $d = 5$ μm, $l = 1.25$ mm | $Nu$ |
| Calibrator for the hot-film/wire probe | TSI, model 1125 | |

### 2.1. Generation of the sound field

Both pairs of transmitters oscillate with a constant frequency of approximately 20 and 10 kHz, respectively. The frequency difference of the two transmitters for each pair is about 100 Hz. Further constant parameters are the ambient temperature $T_a$ (20 °C), the temperature of the hot-film/wire probes (250 °C). The displacement amplitude of the transmitters $Y$ is varied between 30 and 120 μm. The incoming acoustic wave is superimposed with the reflecting wave, if only one transmitter oscillates and the other acts as a reflector. To achieve this, the distance between the two transmitters $L$ has to be $n$ times the half wavelength $\lambda/2$ to generate a standing wave or a resonant acoustic field. In this study, only resonant acoustic fields are considered. A standing wave means that the sound pressure amplitude and the sound particle velocity amplitude remain at a constant position and there is a phase shift of a quarter wavelength $\lambda/4$ between the maxima. This is shown schematically in *figure 3* for one oscillating transmitter. In this case the time-dependent signal (sound pressure/particle velocity) is a simple harmonic oscillation. A beat frequency due to the frequency difference can be observed if the second transmitter is operated in the same way. *Figure 4* qualitatively shows the time-depending signals for one and for two operating

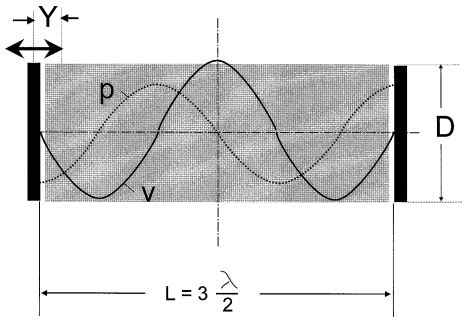


**Figure 3.** Behaviour of sound pressure $p$ and sound particle velocity $v$ in the resonant acoustic field on the $x$-axis (one oscillating transmitter).

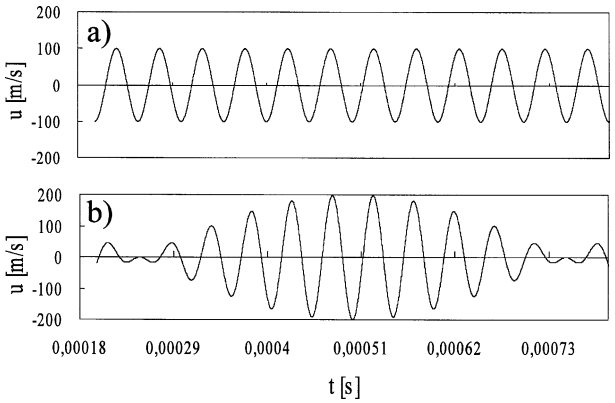


**Figure 4.** Qualitative behaviour of the sound pressure or sound particle velocity in the resonant acoustic field with one (a) and two (b) transmitters in operation.

transmitters. All further results presented in this study are achieved with two active transmitters.

In the following only time-averaged results are shown. All values given below are effective values (root mean square), and it will be pointed out if otherwise.

The distance between the transmitters $L$ may only be a multiple of the half wavelength. Sometimes the distance is given as the number of sound pressure nodes $n$. The experimental setup is located in a pressure vessel so that different gases (air, argon, helium) and ambient pressures $p_a$ can be used.

## 2.2. Sound pressure and sound particle velocity

A piezoelectric probe is used to measure the sound pressure (*table II*). All results given below are effective values on the $x$-axis ($r = 0$) in the sound pressure antinode close to the centre of the acoustic field ($x = \lambda/4$).

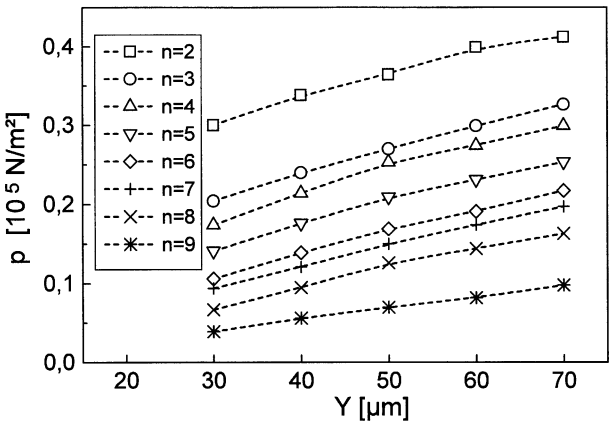


**Figure 5.** Effective sound pressure $p$ over the transmitter amplitude $Y$ with different sound pressure nodes $n$ (air, $p_a = 1{\cdot}10^5$ N·m$^{-2}$, $f = 20$ kHz).

TABLE III
Range of process parameters.

| | | |
|---|---|---|
| Transmitter displacement amplitude | $Y$ | 30–120 µm |
| Sound pressure nodes | $n$ | 1–10 |
| Distance between the transmitters | $L$ | 20–200 mm |
| Speed of sound at normal temperature | $c_0$ | 343 m·s$^{-1}$ in air<br>319 m·s$^{-1}$ in argon<br>1 008 m·s$^{-1}$ in helium |
| Transmitter diameter | $D$ | 35 mm (20 kHz),<br>90 mm (10 kHz) |
| Ambient pressure | $p_a$ | 1–9·10$^5$ N·m$^{-2}$ |
| Oscillation frequency | $f$ | 10 and 20 kHz |

Measurements were carried out with different transmitter displacement amplitudes $Y$, distances between the transmitters $L$ (up to 10 sound pressure nodes $n$) (*figure 5*), ambient pressures, and ambient gases. The different ranges are listed in *table III*.

A smaller number of the measurements were performed with the 10 kHz transmitters. It must be stated that the 10 and 20 kHz transmitters do not have the same dimensions (see *table III*). Furthermore, the distances between the transmitters are different due to the different wavelengths, when the number of pressure nodes is kept constant. The wavelength $\lambda$ and the frequency are linked with the speed of sound $c$ as follows:

$$\lambda = \frac{c}{f} \tag{1}$$

The result for different oscillating frequencies can nevertheless be compared, if the dimensionless number (irradiation number) $\varphi$ is used as a characteristic parameter to represent both the distance $L$ between the transmitters

and the transmitters diameters $D$. The irradiation number defines the exchange of radiation between two planes. The equation given below is valid for two circular planes parallel to each other [20]:

$$\varphi = \frac{1}{2(D/L)^2}\left(1+2\left(\frac{D}{L}\right)^2 - \sqrt{1+4\left(\frac{D}{L}\right)^2}\right) \quad (2)$$

## 2.3. Heat transfer

The hot-film/wire anemometry is a technique which has been used for many years to measure the velocity in laminar flows as well as velocity fluctuations in turbulent flows. The probe is also very well suited for the measurement of heat transfer in oscillating flows. Here the measurement probe and the cylindical test object in the flow are the same. Therefore, the disturbance of the flow due to the probe is negligible. In this study the orientation of the probe axis is perpendicular to the $x$-axis (and horizontal). Therefore, the acoustic field generates an oscillating cross-flow situation. The characteristic length of the probe is $\pi d/2$ (with $d$ being the diameter of the hot-wire probe). The hot-wire probe is made of a thin wire and has a very high frequency response. Generally, hot-wire probes are preferred in comparison to hot-film probes due to the better frequency response and higher accuracy. Their disadvantage is that they are not resistant in high intensive acoustic fields. For this reason, hot-film probes are used in most cases. The probes are calibrated in order to minimize the measuring error. The calibration has been realized in a constant flow. The following equation [21, 22] is used:

$$U^2 - U_0^2 = Bu^m \quad (3)$$

Here $U_0$ means the voltage of the probe under free convection, $U$ is the voltage of the probe under forced convection, and $u$ is the constant gas velocity. The calibration constants $B$ and $m$ are determined by a linear regression.

At the ends of the probe a heat loss arises due to heat conduction to the prongs. Normally, this loss can be neglected for hot-wire probes. In general, the heat loss due to conduction is less than 10 %. However, in the case of a hot-film probe the error is much higher and, therefore, cannot be neglected. The effect can amount to more than 50 % of the total heat transfer of the probe [23]. The energy balance of the probe can be described by

$$P_{\mathrm{el}} = \dot{Q}_{\mathrm{conv}} + \dot{Q}_{\mathrm{cond}} + \dot{Q}_{\mathrm{rad}} \quad (4)$$

However, it can be shown that the heat transfer due to radiation $\dot{Q}_{\mathrm{rad}}$ is always lower than 1 % in this study and, therefore, can be neglected ($\dot{Q}_{\mathrm{rad}} = 0$). Because the electric power $P_{\mathrm{el}}$ can be measured by means of the probe voltage $U$, one obtains an expression for ($\dot{Q}_{\mathrm{conv}} + \dot{Q}_{\mathrm{cond}}$), which can be treated as follows:

$$\dot{Q}_{\mathrm{conv}} = hA(T - T_{\mathrm{a}}) \quad (5)$$

$$P_{\mathrm{el}} = \frac{U^2}{R} \quad (6)$$

with the heat transfer coefficient $h$, the surface area of the probe $A$, the temperature of the probe $T$, the ambient gas temperature $T_{\mathrm{a}}$, and the electric resistance $R$ of the hot wire.

The heat conduction at the ends of the probe is taken into account by using a correction value $\delta = \dot{Q}_{\mathrm{cond}}/(\dot{Q}_{\mathrm{cond}} + \dot{Q}_{\mathrm{conv}})$. This correction value can be derived from the calibration of the probe. The exact procedure is explained by Meng [23]:

$$\delta = 1 - \frac{(0.4 + (0.48d^{0.5}/v^{0.5})((U^2 - U_0^2)/B)^{1/2m})}{U^2/R} \cdot (k/d)(T - T_{\mathrm{a}}) \quad (7)$$

with the gas velocity $v$ and the thermal conductivity $k$. Another approach for the correction value is suggested by Nitsche [24].

Considering Meng's conditions, the equation for the dimensionless convective heat transfer can be described as follows:

$$Nu = (1 - \delta)\frac{U^2}{2klR(T - T_{\mathrm{a}})} \quad (8)$$

with the length of the hot wire $l$.

# 3. RESULTS

## 3.1. Sound pressure and sound particle velocity

A great number of measurements were realized to determine the maximum sound pressure in the acoustic field. The varied parameters are summarized in *table III*. Finally, a regression analysis of the experimental results leads to the following dimensionless equation:

$$\frac{p}{p_{\mathrm{a}}} = 1.03\varphi Y^{*^{0.75}} Z^{*^{0.9}} f^* \quad (x = \lambda/4,\ r = 0) \quad (9)$$

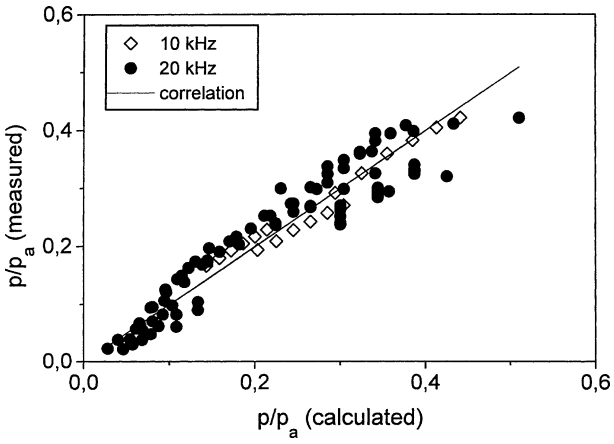


**Figure 6.** Comparison between the measured and calculated normalized sound pressures $p/p_a$.

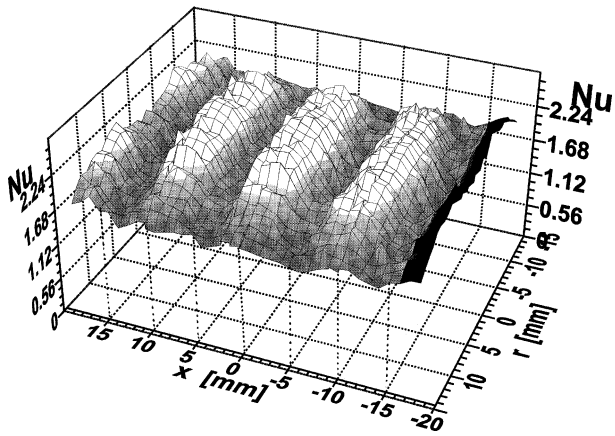


**Figure 7.** Heat transfer in the acoustic field between the two transmitters (hot wire, $Y = 50$ µm, $n = 5$, air, $p_a = 1{\cdot}10^5$ N·m$^{-2}$).

The sound pressure $p$ can be predicted by equation (9), where $p_a$ is the ambient pressure, $\varphi$ is the irradiation number, $Y^*$ is the normalized amplitude of the transmitter ($Y^* = Y/Y_0$, with $Y_0 = 100$ µm), $Z^*$ is the normalized impedance ($Z^* = Z/Z_{air}$), and $f^*$ is the normalized frequency ($f^* = f/f_0$, with $f_0 = 20$ kHz). *Figure 6* shows a comparison between the measured values and the regression analysis. The two symbols stand for different frequencies. The solid line represents the empirical equation (9). The 20 kHz values show higher deviations, but cover a larger pressure range than the 10 kHz values.

The sound particle velocity $v$ in a standing wave can be easily calculated from the sound pressure $p$ and the acoustic impedance $Z$:

$$v = \frac{p}{Z} \quad \text{with } Z = \rho c \tag{10}$$

with the gas density $\rho$.

It should be pointed out that this sound particle velocity $v$ is valid at the center of the acoustic field, whereas the pressure was measured a quarter wavelength away. This is due to the phase shift between the sound pressure and the sound particle velocity, as mentioned above.

## 3.2. Heat transfer

### 3.2.1. Heat transfer in the flow field between the two transmitters

*Figure 7* gives an overview of the heat transfer in the resonant acoustic field. The absolute maximum of heat transfer is located at the center of the acoustic field ($r = 0$ mm, $x = 0$ mm) due to a maximum of the sound particle velocity. There is a strong decrease of the Nusselt number if the center ($r = 0$ mm, $x = 0$ mm) is left in $x$-direction. A minimum of the Nusselt number can be found a quarter wavelength (here approximately $x = 5$ mm) away from the center at the node of the sound particle velocity. Continuing on in $\pm x$-direction there are further maxima. All values are nearly constant in $r$-direction in the range of 10 mm from the center. This result confirms the existence of a plane standing wave between the two transmitters as expected in a resonant acoustic field.

The general features of the results shown in *figure 7* are also valid for other process parameters. Thus, the following results are focused on effects of some of these process parameters. Therefore, instead of scanning the whole acoustic field, it is sufficient to measure at characteristic locations. For this reason the heat transfer has been measured only in the center of the acoustic field ($x, r = 0$), and the sound pressure is measured in the sound pressure antinode close to the center ($x = \lambda/4$).

### 3.2.2. Transmitter amplitude and distance between the transmitters

The effect of the number of nodes (corresponding to the distance between the transmitters) and the amplitude of the transmitter on the heat transfer is presented in *figure 8*. A higher energy input into the acoustic field can be achieved by increasing the amplitude $Y$ of the transmitter. There is nearly a linear increase for higher transmitter amplitudes in the range shown in the figure. An increase of the heat transfer can be observed as well,

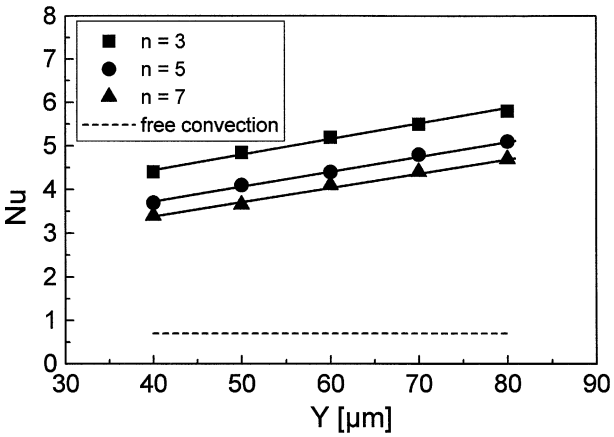


**Figure 8.** Heat transfer at the center of the acoustic field for different transmitter amplitudes $Y$ and sound pressure nodes $n$ (hot film, $p_a = 1{\cdot}10^5$ N·m$^{-2}$, air, $x = r = 0$ mm, $f = 20$ kHz).

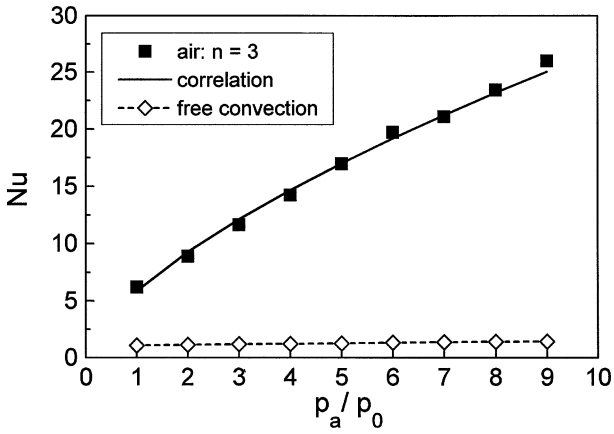


**Figure 9.** Heat transfer as a function of the normalized ambient pressure together with a calculated correlation, compared with the measured value of free convection due to a wire temperature of 250 °C (air, $n = 3$, $Y = 50$ µm, $f = 20$ kHz).

if the distance between the transmitters (less pressure nodes) is smaller. Of course, this could be expected, because the energy loss to the surroundings and ambient gas atmosphere must be smaller, if the distance between the transmitters decreases. In comparison, the dashed line in the figure describes the heat transfer in the case of free convection (without the influence of the acoustic field). The heat transfer in the acoustic field is much higher compared to free convection due to a hot-wire temperature of 250 °C.

### 3.2.3. Ambient pressure

The heat transfer can be enhanced substantially by increasing the ambient pressure. This is shown in *figure 9*. Here the Nusselt number is plotted versus the dimensionless ambient pressure $p_a/p_0$. The experimental results can be expressed by a correlation assuming an exponential law ($Nu \sim (p_a/p_0)^k$), which is shown in the figure as a solid line. Furthermore the experimental results for free convection are shown as well.

Additional measurements are represented in *figure 10* in a more general form. Different gases and distances between the transmitters are taken into account.

It is shown that the results can be described by a single equation, which can be seen in the figure as a dashed line. The correlation given as

$$Nu - Nu_0 = \text{const}\left(\frac{p_a}{p_0}\right)^{0.76} \qquad (11)$$

where $Nu_0$ is the heat transfer for free convection at ambient pressure. The exponent 0.76 refers to the strong effect of the ambient pressure.

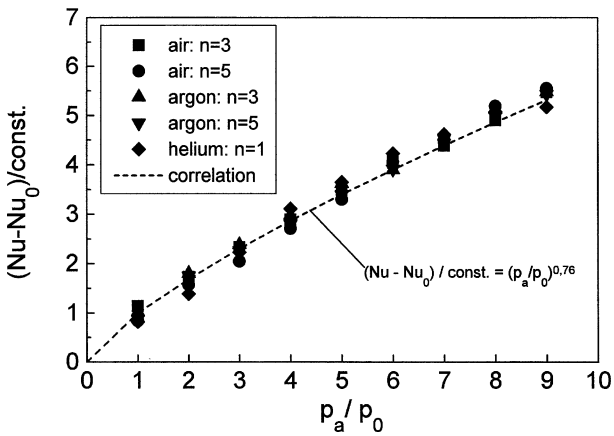


**Figure 10.** Heat transfer in dependency on the normalized ambient pressure for different gases and distances between the transmitters ($Y = 50$ µm, $f = 20$ kHz).

### 3.2.4. Frequency and irradiation number

The heat transfer due to different transmitter frequencies or wavelengths cannot be easily compared because of different geometric transmitter design mentioned above (see equation (1) and *table III*).

The irradiation number is used in order to compensate for the difference in distance between the transmitters and their diameters. Then the velocity amplitude $\hat{v}_{trans}$ of the transmitters must replace the displacement amplitude $Y$. The results are shown in *figure 11*, where the heat transfer is plotted against the irradiation number $\varphi$ with the velocity amplitude and the frequency as parameters. Essentially the heat transfer for 10 and 20 kHz is the same, if it is compared in the overlapped range of the

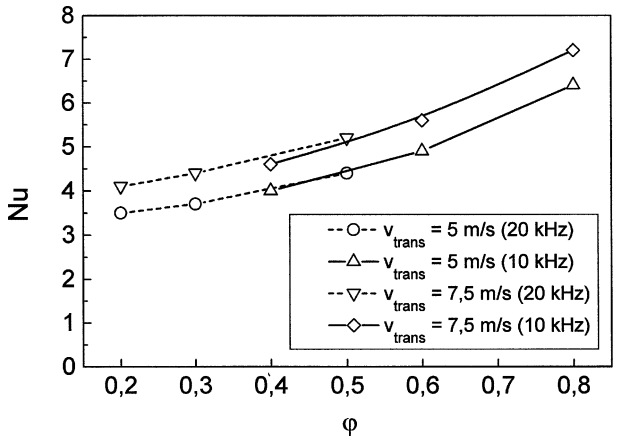


**Figure 11.** Comparison of the heat transfer at different frequencies (hot film, air, $p_a = 1{\cdot}10^5$ N·m$^{-2}$, $r, x = 0$ mm).

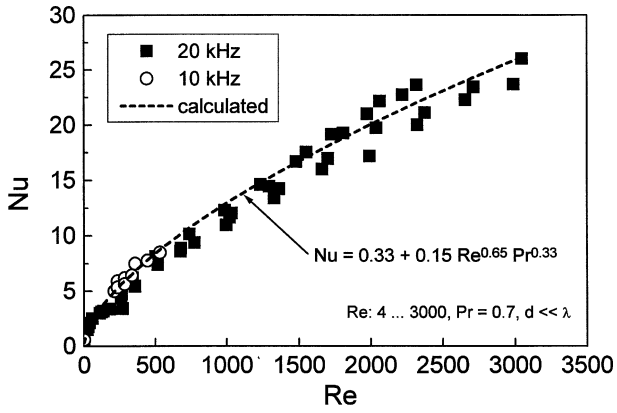


**Figure 12.** Heat transfer *Nu* over the acoustic Reynolds number *Re*, comparison between 10 and 20 kHz.

irradiation number, and for the same velocity amplitudes of the transmitters.

Finally, the heat transfer is shown for all varied parameters versus the acoustic Reynolds number *Re* in *figure 12*. The Reynolds number is defined as follows:

$$Re \equiv \frac{\rho v \pi d/2}{\eta} \tag{12}$$

The different frequencies are marked by different symbols. For the heat transfer an exponential law is assumed, which is often used for cylinders in a constant cross flow:

$$Nu = 0.33 + k_1 Re^{k_2} Pr^{0.33} \tag{13}$$

With the Prandtl number *Pr*, the constant $k_1$ and the exponent $k_2$ are determined for the lower as well as for the higher frequency from the experimental results. Because there exists only a negligible difference between the coefficients, it can be stated that the heat transfer can be described by a single relation (equation (14)), and that the heat transfer does not depend on the frequency:

$$Nu = 0.33 + 0.15 Re^{0.65} Pr^{0.33} \quad \text{with } 4 < Re < 3\,000,$$
$$10\ \text{kHz} \le f \le 20\ \text{kHz},\ d \ll \lambda \tag{14}$$

This relation is shown in *figure 12* as a dashed line. It should be mentioned that the ratio between the characteristic length of the hot-film/wire probes and the wavelength of the standing wave was much smaller than 1. The relation should be used only for the condition $d \ll \lambda$.

## 4. CONCLUSION

The heat transfer from cylindrical bodies in an oscillating, acoustic flow field in a cross-flow situation was investigated in a wide range of Reynolds numbers (4–3 000). Both the frequency range and the intensity (or sound particle velocities) show great differences in comparison to other studies. Parameters such as the transmitter displacement amplitude, the distance between the transmitters, the transmitter diameter, the ambient pressure and the ambient gas were varied. Furthermore, two different frequencies (10 and 20 kHz) were taken into account.

As a result, an empirical equation is given to predict the sound pressure at the antinode of the standing wave in the acoustic field. The heat transfer was determined by using cylindrical hot-film/wire probes located in the acoustic field. Hot-film and hot-wire probes are as well the cylindrical obstacles for the acoustic flow. The heat transfer in the acoustic field could be enhanced by the factor of 25 compared to the value of free convection. Additionally, the investigations lead to a relation, which describes the heat transfer at the center (sound pressure node) of the acoustic field. The equation is valid for Reynolds numbers between 4 and 3 000, and frequencies from 10 to 20 kHz. Finally, the results show no effect of the frequency in the investigated range.

The results are useful for the calculation of the solidification behavior of melts which are atomized due to the sound field. It has already been shown elsewhere that it is possible to produce fine metal powder with a mass median diameter of less than 15 μm by ultrasonic standing wave atomization [9].

Standing wave fields are also used for the levitation of solid particles or liquid droplets in basic research experiments. In this case it is important to know the heat and mass transfer conditions. Due to the similarity of

heat and mass transfer not only the Nusselt number but also the Sherwood number can be predicted from these results.

## REFERENCES

[1] Goldmann G., Waetzmann E., Geschwindigkeitsmessungen mit erhitzten Drähten in stehenden Luftwellen, Z. Phys. 54 (1929) 179–189.

[2] Müller H., Waetzmann E., Absolute Geschwindigkeitsmessungen mit Hitzdrähten in stehenden Schallwellen, Z. Phys. 62 (1930) 449–453.

[3] Trasher B.H., Schaetzle W.J., Instantaneous measurement of heat transfer from an oscillating wire in free convection, J. Heat Tran. 92 (1970) 439–446.

[4] Armaly B.F., Madsen D.H., Heat transfer from an oscillating horizontal wire, J. Heat Tran. 93 (1971) 239–240.

[5] Hutton P., Gammon L.N., Hot films: effects of probe reversal and flow oscillation, J. Phys. E 9 (1979) 921–924.

[6] Elger D.F., Adams R.L., Dynamic hot-wire anemometer calibration using an oscillating flow, J. Phys. E 22 (1989) 166–172.

[7] Bayazitoglu Y., Anderson C., Unsteady heat transfer from spheres at low Reynolds and Strouhal numbers, AIAA Paper No. 93-0915 (1993) 1–10.

[8] Hansmann S., Einfluß von Stoff- und Betriebsparametern auf die Zerstäubung hochviskoser Flüssigkeiten im Ultraschall-Stehwellenfeld, Shaker Verlag, Aachen, 1996.

[9] Andersen O., Feinstzerstäubung von Metallschmelzen mittels der Ultraschall-Stehwellen-Zerstäubung am Beispiel von Zinn, VDI-Verlag, Düsseldorf, 1997.

[10] Uhlenwinkel V., Meng R., Bauckhage K., Andersen O., Schreckenberg P., Heat transfer to cylindrical bodies and small particles in an ultrasonic standig wave field of a melt atomizer, in: Proc. of Multiphase Flow and Heat Transfer in Materials Processing, ASME, FED, Vol. 201, HTD, Vol. 297, Chicago, 1994, pp. 19–24.

[11] Vetters H., Schreckenberg P. Bauckhage K., SEM-analysis of rapid quenched Cu–Ni–P alloy dispersed in an ultrasonic standing wave field, Prakt. Met. 28 (1991) 522–531.

[12] Burdukov A.P., Nakoryakov V.E., Heat transfer from a cylinder in a sound field at Grashof numbers approaching zero, J. Appl. Mech. Techn. Phys. 6 (1965) 112–117.

[13] Larsen P.S., Jensen J.W., Evaporation rates of drops in forced convection with superposed transverse sound field, Int. J. Heat Mass Tran. 21 (1978) 511.

[14] Richardson P.D., Heat transfer from a circular cylinder by acoustic streaming, J. Fluid. Mech. 30 (1967) 337.

[15] Schlichting H., Berechnung ebener periodischer Grenzschichtströmungen, Phys. Z. 33 (1932) 327.

[16] Schlichting H., Gersten K., Grenzschicht-Theorie, Springer-Verlag, 1997, p. 391.

[17] Seaver M., Galloway A., Manuccia T.J., Acoustic lavitation in a free-jet wind tunnel, Rev. Sci. Instrum. 60 (1989) 3452.

[18] Seaver M., Peele J.R., Non-contact fluorescence thermometry of acoustically levitated water drops, Appl. Opt. 29 (1990) 1959.

[19] Tian Y., Apfel R.E., A novel mutiple drop levitatior for the study of drop arrays, J. Aerosol Sci. Am. 79 (1996) 1335.

[20] VDI-Wärmeatlas, 6. Auflage, VDI Verlage, Düsseldorf, 1991.

[21] Freymuth P., Thermal Anemometry, Instrumentation and Analysis, Cheremisinoff P.N. (Ed.), Ann Arbor Science, New Jersey, 1989.

[22] King L.V., On the convection of heat from small cylinders in a stream of fluid, Proc. Roy. Soc. Ser. A 214 (1914) 14–19.

[23] Meng R.X., Untersuchungen zum Wärmeübergang in unterschiedlichen Konfigurationen von Ultraschallfeldern, u.a. zur Zerstäubung metallischer Schmelzen, Ph.D. Thesis, Universität Bremen, Germany, 1997.

[24] Nitsche W., Haberland C., U. Flugwiss. Weltraumforschung 4 (1984).

[25] Bremhorst K., Gilmore D.B., Comparison of dynamic and static hot wire anemometer calibrations for velocity perturbation measurements, J. Phys. E 9 (1976) 1097–1100.

[26] Fand R.M., Cheng P., The influence of sound on heat transfer from a horizontal cylinder, J. Heat Mass Tran. 6 (1962) 571–595.

[27] Sreenivasan K., Ramachandran A., Effect of vibration on heat transfer from a horizontal cylinder to a normal air stream, Int. J. Heat Mass Tran. 3 (1960) 60–67.

[28] Woods B.G., Sonically enhanced heat transfer from a cylinder in cross flow and its impact on process power consumption, Int. J. Heat Mass Tran. 35 (1992) 2367–2375.

[29] Baxi C.B., Ramachandran A., Effect of vibration on heat transfer from spheres, J. Heat Tran. 8 (1969) 337–344.